coatings

MDPI

Communication

$Nd_2Fe_{14}B$/FeCo Core–Shell Nanoparticle Synthesis Using Galvanic Substitution Based Electroless Plating

Muhammad Aneeq Haq [1,2,†], Han-Saem Lee [2,†], Mi Hye Lee [2], Da-Woon Jeong [2], Eom Nu Si A [3], Bin Lee [2], Yoseb Song [2,*] and Bum Sung Kim [1,2,*]

1 Industrial Technology, University of Science and Technology, Daejeon 34113, Korea; aneeqhaq@ust.ac.kr
2 Korea Institute of Industrial Technology, Incheon 21999, Korea; sol940721@gmail.com (H.-S.L.); lmh62@kitech.re.kr (M.H.L.); t-dwjeong@kitech.re.kr (D.-W.J.); lbin@kitech.re.kr (B.L.)
3 Korea Electronics Technology Institute, Seongnam 13509, Korea; djafntldk@hanmail.net
* Correspondence: bskim15@kitech.com (Y.S.); songys88@kitech.re.kr (B.S.K.)
† These authors contributed equally to this work.

Abstract: Core–shell structured magnetic nanoparticles combine hard and soft phases to improve energy efficiency. The mutual interaction of the two phases can lead to the exchange spring effect, leading to higher magnetic energy. In this regard, synthesis of $Nd_2Fe_{14}B$-based core–shell-structured powders have proven to be elusive, due to the relatively reactive nature of this phase. In this study, a process has been established for successfully coating the surface of $Nd_2Fe_{14}B$ powders with a FeCo layer using the galvanic displacement method. Initially, a binary phase magnetic powder was synthesized containing $Nd_2Fe_{14}B$ and Nd_2Fe_{17} phase. Subsequently, the powders were coated using a Co precursor at 303 K. During coating, the metastable Nd_2Fe_{17} phase was dissolved, and the Fe ions were released into the solution. Subsequently, the Fe ions deposited together with the Co ions on the surface of $Nd_2Fe_{14}B$ powder to form a FeCo shell. The deposited layer thickness and composition was confirmed using TEM analysis.

Keywords: $Nd_2Fe_{14}B$; FeCo; core–shell structure; galvanic substitution; electroless plating

Citation: Haq, M.A.; Lee, H.-S.; Lee, M.H.; Jeong, D.-W.; Si A, E.N.; Lee, B.; Song, Y.; Kim, B.S. $Nd_2Fe_{14}B$/FeCo Core–Shell Nanoparticle Synthesis Using Galvanic Substitution Based Electroless Plating. *Coatings* **2022**, *12*, 389. https://doi.org/10.3390/coatings12030389

Academic Editor: Joaquim Carneiro

Received: 13 January 2022
Accepted: 23 February 2022
Published: 15 March 2022

1. Introduction

Core–shell structured powders are a special class of materials having multifunctional properties [1–6]. This unique powder structure allows for a convenient superimposition of the core and shell phase properties [5,6]. Owing to their high functionality, core–shell-structured powders have been developed for a wide range of applications, including magnets [7–11], semiconductors [12], organic/inorganic composites [13,14], and metal matrix composites [5,15]. These specialized materials have allowed the researchers to go beyond the property limits of traditional single phase materials [5]. In particular, core–shell-structured magnetic nanoparticles have the potential to achieve enhanced magnetic energy product [8]. This enhancement effect, known as the exchange-spring magnetic effect, is caused by the mutual interaction of hard and soft magnetic phases [16]. The exchange-spring effect has been successfully demonstrated on several hard magnetic systems, including Nd-Fe-B [7], Sm-Co [8], Fe-Pt [10] and various ferrites [11]. These studies give ample evidence for the immense potential of spring magnets as highly energy-efficient materials.

Theoretically, the $Nd_2Fe_{14}B$-based magnets are the most suitable material system for obtaining spring magnets. Atomistic studies and finite element simulations have revealed the superior potential of the $Nd_2Fe_{14}B$-based core–shell powders in realizing the maximum magnetic energy [17,18]. However, given the complexity of the $Nd_2Fe_{14}B$ crystal structure, the fabrication of such powder with a uniform soft magnetic coating is challenging. Therefore, despite the encouraging results in other magnetic systems, no such successful attempt obtaining core–shell-structured $Nd_2Fe_{14}B$ powder has been reported. In

this regard, there is an imminent need for developing a coating technique for obtaining an $Nd_2Fe_{14}B$ powder coated with a soft magnetic shell.

Here, we report the development of a novel process for synthesizing $Nd_2Fe_{14}B$ powder coated with a FeCo layer. Initially a nanostructured $Nd_2Fe_{14}B$ powder containing a metastable Nd_2Fe_{17} phase was fabricated by electrospinning, calcination and reduction of Nd, Fe and B precursors. Afterwards the electroless plating of the prepared powder was performed in a Cobalt (Co) bath. During the plating process, the galvanic substitution of the metastable Nd_2Fe_{17} phase was performed to ionize Fe while preserving the $Nd_2Fe_{14}B$ phase. Concomitantly, the Fe ions were co-deposited along with Co on the surface of $Nd_2Fe_{14}B$. Finally, the formation of the FeCo layer was confirmed.

2. Materials and Methods

The starting $Nd_2Fe_{14}B$ powder was synthesized via electrospinning, calcination, reduction and washing process. Initially fibers were obtained by electrospinning of a Polyvinylpyrrolidone (PVP, M_w~1,300,000, Sigma-Aldrich Inc., St. Louis, MO, USA) solution containing Nd, Fe and B precursors in an electrospinning machine (NSLAB, Elmarco). The resultant fibers were calcined in air to obtain Nd-Fe-B oxide fibers and remove the PVP. Afterwards, the oxide fibers were reduced in an argon atmosphere using Calcium (Ca) granules at 1123 K. Finally, the reduced fibers were broken down into powder during washing. The detailed description of each step can be found elsewhere [19].

As a pretreatment before the FeCo coating, the hard magnetic powder was washed in methanol followed by the surface sensitization and activation treatments. Tin chloride dihydrate ($SnCl_2{\cdot}2H_2O$, 98%, Sigma-Aldrich Inc., St. Louis, MO, USA) and palladium chloride ($PdCl_2$, 99%, Sigma-Aldrich Inc., St. Louis, MO, USA) were used for the sensitization and activation treatment, respectively. The sensitization and activation treatments were performed in an aqueous solution containing HCl at room temperature for 0.5 and 10 min, respectively. Finally, the powder was electroplated in a cobalt bath for obtaining a FeCo coating. The composition of the electroless plating solution was 0.09 M cobalt sulfate heptahydrate ($CoSO_4{\cdot}7H_2O$, 99%, Sigma-Aldrich Inc., St. Louis, MO, USA), 0.25 M sodium hypophosphite monohydrate ($NaH_2PO_2{\cdot}H_2O$, Alfa Aesar Co., Kandel, Germany), 0.3 M sodium citrate dihydrate ($Na_3C_6H_5O_7{\cdot}2H_2O$, 99%, Thermo-Fisher Inc., Waltham, MA, USA), and 0.1 M diammonium sulfate ($(NH_4)_2SO_4$, 99%, Sigma-Aldrich Inc., St. Louis, MO, USA). The plating process was performed at a temperature of 303 K for 10 min, and the pH was kept at 9 using an aqueous solution of sodium hydroxide (NaOH, 93%, Duksan Co., Gyeonggi-do, Korea) having a concentration of 2 M.

The phase change, microstructure and composition of the powders were analyzed using X-ray diffraction analyzer (XRD, D-8 Advanced, Bruker), scanning electron microscope (FE-SEM, JSM-7100F, JOEL), energy dispersive X-ray spectroscopy (EDX, Oxford Instruments), and transmission electron microscope (TEM, JEM-2100F, JEOL). The shell formation mechanism was analyzed through primary particle analysis. The average particle size and deviation were calculated by analyzing 50 particles using the ImageJ program.

3. Results

The morphological changes during each step of $Nd_2Fe_{14}B$ powder synthesis are shown in Figure 1. After the electrospinning step, the obtained polymeric fiber had a smooth surface with a diameter of around 750 $\pm$ 50 nm (Figure 1a). Upon calcination, the diameter of the fibers reduced to 550 $\pm$ 100 nm as the water and PVP were removed (Figure 1b). A high degree of porosity is visible in the calcined oxide fibers. The polymer to precursor ratio used for electrospinning was kept high to induce porosity within the fibers after calcination [20]. As a result, these fibers can be easily converted into nanosized powder during the subsequent processing. Figure 1c shows the fiber morphology after reduction treatment in the presence of Ca granules. The Ca reacts with the oxide fibers and deposits on the fiber surface and within the pores in the form of CaO. The diameter at this stage increased to 900 $\pm$ 200 nm. Finally, the reduced sample was washed in an NH_4Cl solution to

remove the CaO from the sample. The washing solution was chosen due to the effectiveness in removing CaO while preserving the magnetic powder [21].

The fibrous structure broke down during the washing step and nanosized powder was obtained. Figure 1d shows the resultant powders obtained by using ultrasonication of the washed sample. The finally obtained powder had an average particle size of 252 ± 38 nm. However, the nanosized powder particles were present in the form of agglomerates. Table 1 shows the fiber shape diameter information and the particle size analysis results of the nanocomposite powder.

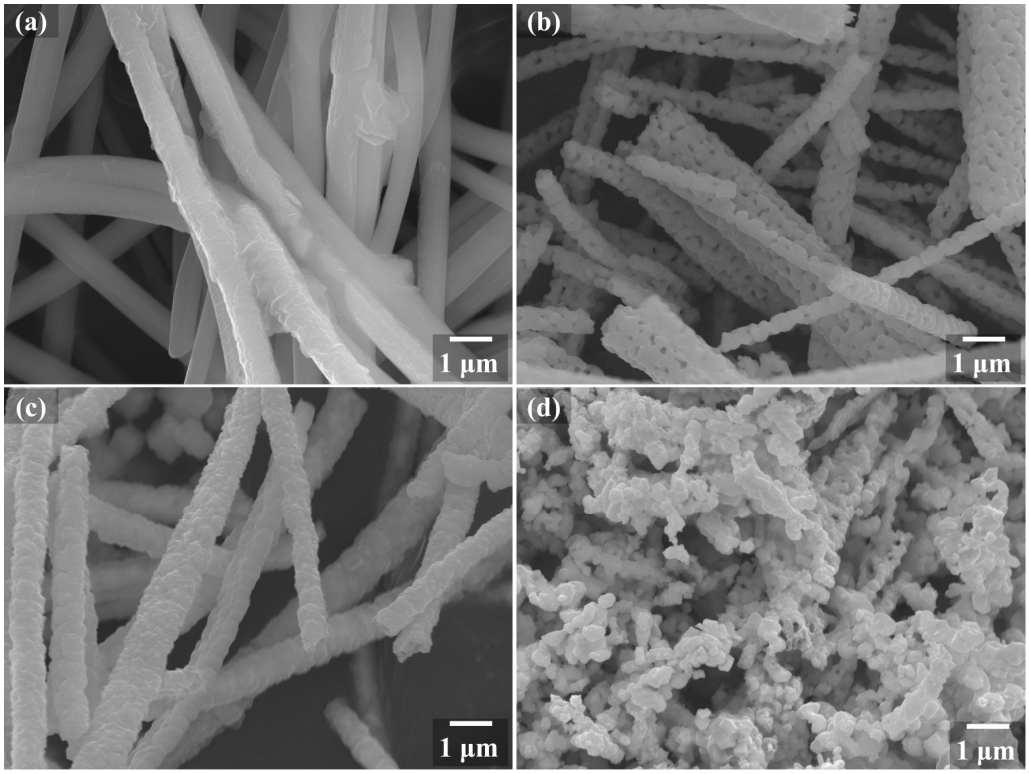

Figure 1. Micrographs of $Nd_2Fe_{14}B$ nanoparticle fabrication process after each stage: (**a**) as spun, (**b**) calcined, (**c**) reduced and (**d**) washed.

Table 1. Measured diameters of the sample at each process stage.

Process	As Spun	Calcined	Reduced	Washed	Pre-Treated	Deposited
Fiber diameter (nm)	750	550	900	-	-	-
Particle diameter (nm)	-	-	-	252	249	254
Distribution (±nm)	50	100	200	39	32	47

The powder obtained after washing and ultrasonication was pretreated in Sn and Pd solutions for sensitization and activation, respectively. This treatment is necessary for enhancing the deposition rate by activating the powder surface [22]. Figure 2a shows the SEM and EDX mapping of the pretreated powder. The powder size and morphology of the pretreated powder remained similar to the as synthesized powder. The powder size was measured to be around 249 ± 32 nm. The EDX maps in Figure 2a show a relatively uniform distribution of Pd while some evidence of unreacted Sn can be observed. This can be caused by inherent agglomeration of the nanosized powder which provides pockets for unreacted Sn deposition [8].

After the pretreatment, the resultant powders were treated in Co bath for obtaining FeCo coating on the powder surface. After 10 min of plating, the process was stopped and the powders were filtered, rinsed and dried. Figure 2b shows the SEM and EDX mapping of the powder after electroless plating step. The size of the coated powder was measured to be 254 ± 47 nm. However, the difference in size between pre-coated and coated powder was statistically insignificant. The EDX analysis confirmed a uniformly distributed presence of Co on the powder surface. This confirmed the successful plating of Co onto the powder surface. Further analysis using XRD was conducted to confirm the phase changes.

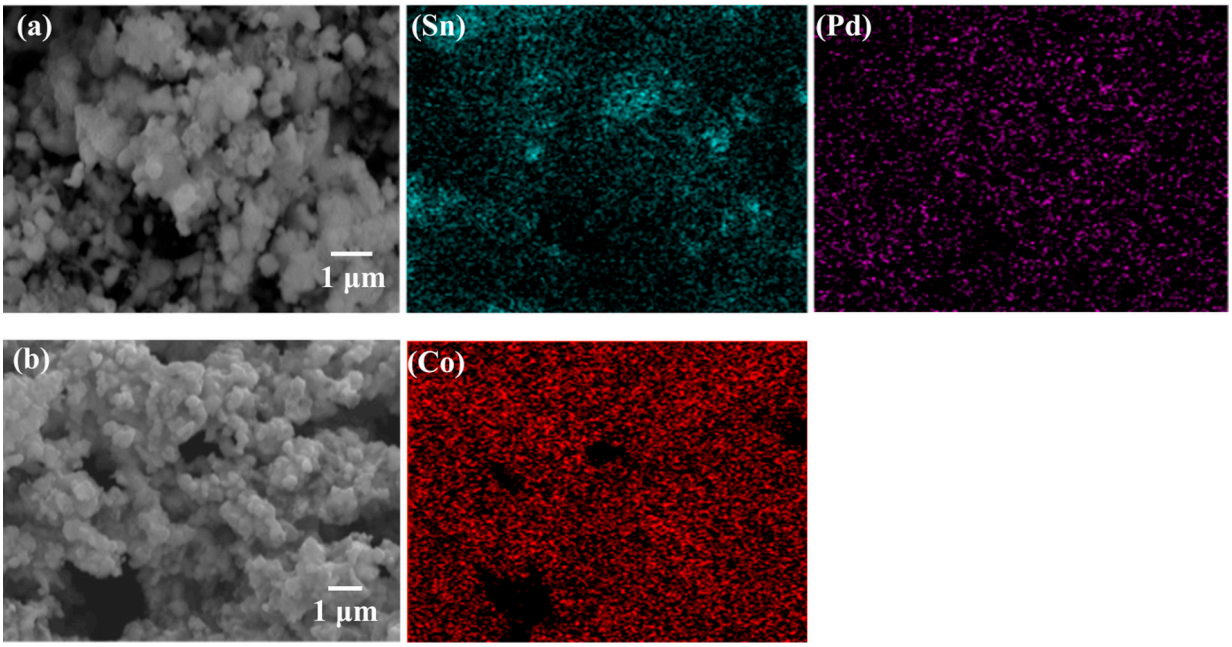

Figure 2. (**a**) SEM along with EDX mapping images of pre-treated Nd-Fe-B powder; (**b**) SEM along with EDX mapping images of the Co deposited powder.

The XRD analysis of the washed, pretreated and plated sample was carried out to confirm the phase composition of the powder. The XRD patterns are shown in Figure 3. The XRD pattern of the as-prepared powder, represented by the black line, consisted of a main $Nd_2Fe_{14}B$ phase along with secondary phases of Nd_2Fe_{17} and α-Fe. The presence of secondary phase is inherent within the adapted synthesis procedure. It has been previously reported that the fiber is made up of a Fe_2O_3, $FeNdO_3$ and $NdBO_3$ composite after the calcination step [23]. During the reduction, the composite oxide fibers reduce together to form $Nd_2Fe_{14}B$. However, by reducing the boron content within the oxide fibers, the presence of Nd_2Fe_{17} and α-Fe phases can be induced [24].

The primary α-Fe phase peak at 44.8° can be clearly seen in the zoom-in image of this region (Figure 3b). In the XRD pattern of the sensitized and activated powder, represented by the red line, the α-Fe peaks were greatly reduced. The low pH of 1–2 used during pretreatment caused the dissolution of excess α-Fe while only $Nd_2Fe_{14}B$ and Nd_2Fe_{17} peaks remain. Koyama et al. reported the superior chemical stability of Nd as compared to Fe under various pH values [25]. It was shown that the Fe phase selectively ionized Fe^{2+} by leaving out Nd_2Fe_{17} and $Nd_2Fe_{14}B$ in the solution. Given below is the chemical equation of Fe ionization during the pretreatment process:

$$Fe + HCl_{(l)} \rightarrow FeCl_{2(aq)} + H_{2(g)} \quad (1)$$

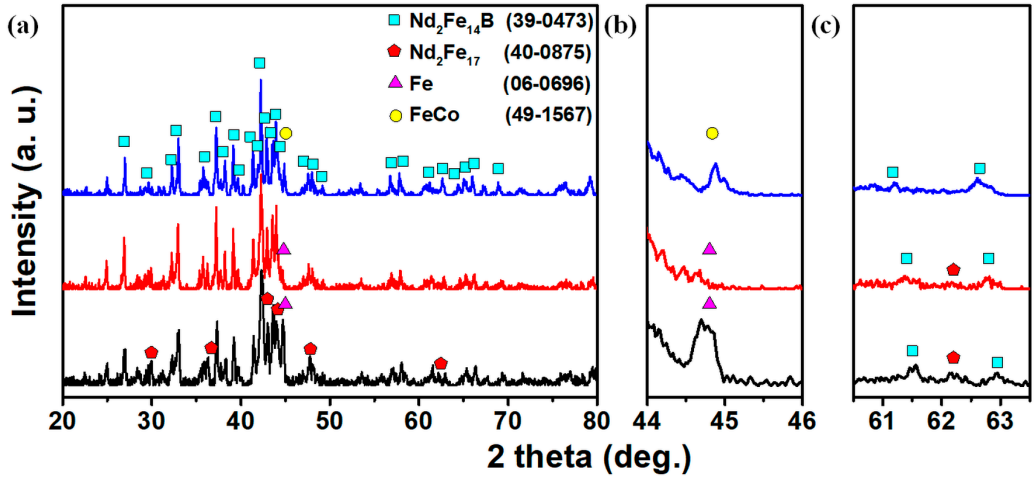

Figure 3. (**a**) XRD patterns of the washed (black), pre-treated (red) and plated (blue) samples. (**b**) Zoom-in XRD image showing enlarged Fe and FeCo peaks. (**c**) Zoom-in XRD image showing enlarged Nd_2Fe_{17} and $Nd_2Fe_{14}B$ peaks.

Finally, the XRD pattern of the plated powder, represented by the blue line, shows a reappearance of the same peak. This peak can be attributed the deposited BCC FeCo phase as no separate Co peaks are observed alongside. The BCC FeCo phase has a lattice parameter of 0.2856 nm. Based on the lattice parameter, the atomic percentage of Fe within the FeCo can be predicted using the following Equation [26]:

$$a = 0.2836 + 0.000064514 \times [at.\%\mathrm{Fe}]/\mathrm{nm} \quad (2)$$

where '*a*' is the lattice parameter of the BCC phase. Using Equation (2), the Fe atomic concentration in FeCo was calculated to be 51.7%.

The primary peaks of Nd_2Fe_{17} peaks are difficult to separate from the $Nd_2Fe_{14}B$ peaks due to the strong overlap between the two phases. Figure 3c shows the distinct peaks of these phases at larger diffraction angles. The peaks of $Nd_2Fe_{14}B$ remain visible in all three samples whereas the Nd_2Fe_{17} peak disappears after electroless plating. Thermodynamically, the Nd_2Fe_{17} is a metastable phase which forms under non-equilibrium conditions whereas the $Nd_2Fe_{14}B$ is more stable [27]. As a result, during the electroless plating, Nd_2Fe_{17} preferentially dissociates while $Nd_2Fe_{14}B$ phase is retained.

As the FeCo phase and α-Fe have a similar XRD pattern, it is difficult to distinguish between the two to confirm the composition of the coated phase. The TEM analysis of the powder surface was conducted to further verify the elemental composition and observe the layer thickness. Figure 4 shows TEM image superimposed with an EDX line map of electroless plated $Nd_2Fe_{14}B$ powder.

A thin layer of under 6.4 nm thickness can be observed at the powder surface. The distinct regions in Figure 4 are marked using a dotted yellow line. The white arrow indicates the interface between core and shell, while the red arrow indicates the powder surface. There is a clear interface present between the core and the shell phase, which can be identified by the initial detection of the Nd signal. In the EDX line map, from the shell region denoted by (2), signals of both Fe and Co can be confirmed. As the line moves into the core region denoted by (1), the Nd and Fe signals increase while the Co signal becomes stable. The Co concentration is even observed within the core as the powder is encapsulated by a FeCo shell. The EDX result confirms the formation of a core–shell structure formation between hard and soft magnetic phases. The thickness of the soft phase is sufficiently thin for developing exchange spring magnetic effect [16].

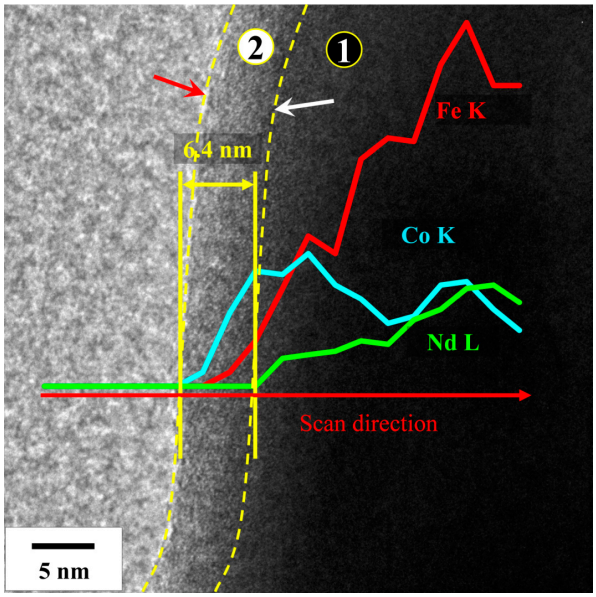

Figure 4. TEM image along with EDX line map taken from surface of the plated powder.

The formation of FeCo layer as well as the preservation of the $Nd_2Fe_{14}B$ phase confirms that the galvanic substitution progressed at the expense of Nd_2Fe_{17} during the plating process. The reported results confirm the possibility of obtaining soft phase coating on $Nd_2Fe_{14}B$ permanent magnetic powder by careful design of the reaction process. Based on these promising initial results, additional fine tuning will be carried out to attain a powder with ideal exchange spring magnetic effect. The content of the metastable phase needs to be adjusted to increase the Fe concentration within the shell phase. Additionally, the agglomeration of the nanosized powder needs to be controlled for obtaining a thorough coating of the shell phase around each individual $Nd_2Fe_{14}B$ particle.

4. Conclusions

Electroless plating of a soft magnetic FeCo phase on a hard magnetic $Nd_2Fe_{14}B$ nanoparticles has been successfully reported. The starting nanocomposite hard magnetic powder was synthesized using a modified electrospinning technique. The powder consisted of a primary $Nd_2Fe_{14}B$ phase along with a secondary phase of metastable Nd_2Fe_{17} phase. The starting powder surface was then subjected to sensitization and activation treatment followed by electroless plating in a Co bath. During the electroless plating, the Nd_2Fe_{17} phase preferentially ionized leaving behind only $Nd_2Fe_{14}B$ powder. Consequently, the ionized Fe from the Nd_2Fe_{17} phase co-deposited along with Co on to the surface of $Nd_2Fe_{14}B$ powder to form a soft magnetic shell. The XRD and TEM analysis confirmed that the deposited shell was of FeCo phase while the core was of $Nd_2Fe_{14}B$ phase. The thickness of the shell was measured to be 6.4 nm. The designed process opens up a vital avenue for developing $Nd_2Fe_{14}B$-based spring magnetic materials which can possess unmatched magnetic energy product. Further research needs to be conducted for tuning the structural and compositional features of the shell to obtain optimal magnetic properties.

Author Contributions: Conceptualization, H.-S.L. and Y.S.; methodology, H.-S.L. and E.N.S.A.; validation, M.H.L., E.N.S.A. and B.S.K.; formal analysis, H.-S.L. and Y.S.; investigation, H.-S.L.; resources, B.L. and B.S.K.; data curation, M.A.H. and D.-W.J.; writing—original draft preparation, M.A.H. and Y.S.; writing—review and editing, M.A.H., M.H.L., D.-W.J. and Y.S.; visualization, M.A.H.; supervision, M.A.H. and D.-W.J.; project administration, D.-W.J. and Y.S.; funding acquisition, B.L. and B.S.K. All authors have read and agreed to the published version of the manuscript.

Funding: This study was performed with the support of Korea Institute of Industrial Technology titled "Development of manufacturing technology for nano-tungsten and carbide materials for tools

with Korea-Uzbekistan Scientific Technology Center on Rare Metals and Hard alloys" Project number JE220008.

Institutional Review Board Statement: Not Applicable.

Informed Consent Statement: Not Applicable.

Data Availability Statement: The data supporting the reported results can be requested from the corresponding author (B.S.K.).

Conflicts of Interest: The authors declare no conflict of interest. The funders had no role in the design of the study, in the collection, analyses, or interpretation of data, in the writing of the manuscript, or in the decision to publish the results.

References

1. Chaudhuri, R.G.; Paria, S. Core/Shell Nanoparticles: Classes, Properties, Synthesis Mechanisms, Characterization, and Applications. *Chem. Rev.* **2012**, *112*, 2373–2433. [CrossRef] [PubMed]
2. Gawande, M.B.; Goswami, A.; Asefa, T.; Guo, H.; Biradar, A.V.; Peng, D.-L.; Zboril, R.; Varma, R.S. Core–Shell Nanoparticles: Synthesis and Applications in Catalysis and Electrocatalysis. *Chem. Soc. Rev.* **2015**, *44*, 7540–7590. [CrossRef] [PubMed]
3. Min, Y.; Song, G.; Zhou, L.; Wang, X.; Liu, P.; Li, J. Silver@mesoporous Anatase TiO_2 Core-Shell Nanoparticles and Their Application in Photocatalysis and SERS Sensing. *Coatings* **2022**, *12*, 64. [CrossRef]
4. Guo, W.; Zhang, H.; Zhao, S.; Ding, Z.; Liu, B.; Li, W.; Xu, H.; Liu, H. Corrosion Behavior of the CoNiCrAlY-Al2O3 Composite Coating Based on Core-Shell Structured Powder Design. *Materials* **2021**, *14*, 7093. [CrossRef] [PubMed]
5. Haq, M.A.; Song, Y.; Lee, H.; Khalid, M.W.; Jeong, D.-W.; Park, K.-R.; Kim, B.S. An In-Situ Approach for Fabricating Network Reinforced CoCrFeNi Matrix Composite. *Mater. Sci. Eng. A* **2021**, *818*, 141405. [CrossRef]
6. Ji, S.M.; Tiwari, A.P.; Kim, H.Y. Graphene Oxide Coated Zinc Oxide Core–Shell Nanofibers for Enhanced Photocatalytic Performance and Durability. *Coatings* **2020**, *10*, 1183. [CrossRef]
7. Li, H.; Li, X.; Guo, D.; Lou, L.; Li, W.; Zhang, X. Three-Dimensional Self-Assembly of Core/Shell-Like Nanostructures for High-Performance Nanocomposite Permanent Magnets. *Nano Lett.* **2016**, *16*, 5631–5638. [CrossRef]
8. Lee, J.; Kim, J.; Kim, D.; Lee, G.; Oh, Y.-B.; Hwang, T.-Y.; Lim, J.-H.; Cho, H.-B.; Kim, J.; Choa, Y.-H. Exchange-Coupling Interaction in Zero- and One-Dimensional Sm_2Co_{17}/FeCo Core–Shell Nanomagnets. *ACS Appl. Mater. Interfaces* **2019**, *11*, 26222–26227. [CrossRef]
9. Li, X.; Lou, L.; Song, W.; Huang, G.; Hou, F.; Zhang, Q.; Zhang, H.-T.; Xiao, J.; Wen, B.; Zhang, X. Novel Bimorphological Anisotropic Bulk Nanocomposite Materials with High Energy Products. *Adv. Mater.* **2017**, *29*, 1606430. [CrossRef]
10. Zhang, W.; Yang, W.; Chandrasena, R.U.; Özdöl, V.B.; Ciston, J.; Kornecki, M.; Raju, S.; Brennan, R.; Gray, A.X.; Ren, S. The Effect of Core–Shell Engineering on the Energy Product of Magnetic Nanometals. *Chem. Commun.* **2018**, *54*, 11005–11008. [CrossRef]
11. Dong, J.; Zhang, Y.; Zhang, X.; Liu, Q.; Wang, J. Improved Magnetic Properties of $SrFe_{12}O_{19}$/FeCo Core–Shell Nanofibers by Hard/Soft Magnetic Exchange–Coupling Effect. *Mater. Lett.* **2014**, *120*, 9–12. [CrossRef]
12. Reiss, P.; Protière, M.; Li, L. Core/Shell Semiconductor Nanocrystals. *Small* **2009**, *5*, 154–168. [CrossRef] [PubMed]
13. Naderi, N.; Sharifi-Sanjani, N.; Khayyat-Naderi, B.; Faridi-Majidi, R. Preparation of Organic–Inorganic Nanocomposites with Core-Shell Structure by Inorganic Powders. *J. Appl. Polym. Sci.* **2006**, *99*, 2943–2950. [CrossRef]
14. Jia, H.; Quan, T.; Liu, X.; Bai, L.; Wang, J.; Boujioui, F.; Ye, R.; Vlad, A.; Lu, Y.; Gohy, J.-F. Core-Shell Nanostructured Organic Redox Polymer Cathodes with Superior Performance. *Nano Energy* **2019**, *64*, 103949. [CrossRef]
15. Haq, M.A.; Eom, N.S.A.; Su, N.; Lee, H.; Kim, T.S.; Kim, B.S. Powder Interface Modification for Synthesis of Core-Shell Structured CoCrFeNiTi High Entropy Alloy Composite. *Appl. Surf. Sci.* **2020**, *506*, 144925. [CrossRef]
16. Kneller, E.F.; Hawig, R. The Exchange-Spring Magnet: A New Material Principle for Permanent Magnets. *IEEE Trans. Magn.* **1991**, *27*, 3588–3600. [CrossRef]
17. Westmoreland, S.C.; Skelland, C.; Shoji, T.; Yano, M.; Kato, A.; Ito, M.; Hrkac, G.; Schrefl, T.; Evans, R.F.L.; Chantrell, R.W. Atomistic Simulations of α-Fe/Nd2Fe14B Magnetic Core/Shell Nanocomposites with Enhanced Energy Product for High Temperature Permanent Magnet Applications. *J. Appl. Phys.* **2020**, *127*, 133901. [CrossRef]
18. Bance, S.; Oezelt, H.; Schrefl, T.; Winklhofer, M.; Hrkac, G.; Zimanyi, G.; Gutfleisch, O.; Evans, R.F.L.; Chantrell, R.W.; Shoji, T.; et al. High Energy Product in Battenberg Structured Magnets. *Appl. Phys. Lett.* **2014**, *105*, 192401. [CrossRef]
19. Eom, N.S.A.; Jeon, E.J.; Haq, M.A.; Lee, J.; Choa, Y.-H.; Kim, B.S. Fabrication and Characterization of 1-Dimensional Neodymium-Iron-Boron Fibers Using New Reduction-Diffusion Process. *Mater. Lett.* **2020**, *268*, 127611. [CrossRef]
20. Eom, N.S.A.; Noh, S.; Haq, M.A.; Kim, B.S. Synthesize of $Nd_2Fe_{14}B$ Powders from 1-D $Nd_2Fe_{14}B$ Wires using Electrospinning Process. *J. Korean Powder Metall. Inst.* **2019**, *26*, 477–480. [CrossRef]
21. Lee, J.; Hwang, T.-Y.; Cho, H.-B.; Kim, J.; Choa, Y.-H. Near Theoretical Ultra-High Magnetic Performance of Rare-Earth Nanomagnets via the Synergetic Combination of Calcium-Reduction and Chemoselective Dissolution. *Sci. Rep.* **2018**, *8*, 15656. [CrossRef] [PubMed]
22. Gulla, M.; Conlan, W.A. Catalyst Solution for Electroless Deposition of Metal on Substrate 1975. US Patent 3874882A, 1 April 1975.

23. Jeon, E.J.; Eom, N.S.A.; Choa, Y.-H.; Kim, B.S. Synthesis of One-Dimensional Neodymium-Iron-Boron-Oxides. *Mater. Lett.* **2020**, *264*, 127286. [CrossRef]
24. Sun, A.-z.; Wu, S.; Xu, W.-h.; Wang, J.; Zhang, Q.; Zhai, F.-Q.; Volinsky, A.A. Nd_2Fe_{17} nanograins effect on the coercivity of HDDR NdFeB magnets with low boron content. *Int. J. Miner. Metall. Mater.* **2012**, *19*, 236–239. [CrossRef]
25. Tanaka, M.; Oki, T.; Koyama, K.; Narita, H.; Oishi, T. Chapter 255-Recycling of Rare Earths from Scrap. In *Handbook on the Physics and Chemistry of Rare Earths*; Bünzli, J.-C.G., Pecharsky, V.K., Eds.; Including Actinides; Elsevier: Amsterdam, The Netherlands, 2013; Volume 43, pp. 159–211.
26. Ohnuma, I.; Enoki, H.; Ikeda, O.; Kainuma, R.; Ohtani, H.; Sundman, B.; Ishida, K. Phase Equilibria in the Fe–Co Binary System. *Acta Mater.* **2002**, *50*, 379–393. [CrossRef]
27. Van Ende, M.-A.; Jung, I.-H. Critical Thermodynamic Evaluation and Optimization of the Fe–B, Fe–Nd, B–Nd and Nd–Fe–B Systems. *J. Alloy. Compd.* **2013**, *548*, 133–154. [CrossRef]